Mars Powered Descent Phase Guidance Design Based on Fixed-time Stabilization Technique

Yao Zhang, Ranjan Vepa, *Member, IEEE,* Guang Li, *Member, IEEE,* and Tianyi Zeng

***Abstract*—This paper proposes a guidance scheme to achieve an autonomous precision landing on Mars and proposes a practical fixed-time stabilization theorem to analyze the robustness of the guidance. The proposed guidance is mainly based on the fixed-time stabilization method, and it can achieve the precision landing within a pre-defined time. This property enables the proposed guidance to outperform the finite-time stabilization technique which cannot handle uncertainties well and whose convergence time is dependent on initial states. Compared with the existing fixed-time stabilization theorem, the proposed practical fixed-time stabilization theorem can achieve a shorter convergence time and cope with unknown disturbances. When the Mars landing guidance is designed by this proposed theorem, the upper bound of the landing time and the maximum landing error subject to unknown disturbances can be calculated in advance. Theoretical proofs and Monte Carlo simulation results confirm the effectiveness of the proposed theorem and the proposed guidance. Furthermore, the efficacy of the proposed guidance with thrust limitations is also demonstrated by testing of 50 cases with a range of initial positions and velocities.**

***Index Terms*—Mars landing missions, practical fixed-time stabilization, multiple sliding surface, powered descent phase, disturbance rejection, control input saturation**

I. Introduction

Several Mars landing missions, such as Viking, Spirit, Opportunity, and Phoenix have been completed. For the next generation missions, the problem of landing at a precise, pre-specified point has been widely studied in recent years [20]. The process of Mars landing is generally divided into three stages, i.e. the entry, descent, and landing (EDL) [26]. For a precision landing mission, the powered descent phase is the final stage of the whole landing mission, which determines the landing accuracy.

Several methodologies have been adopted to design guidance algorithms for the powered descent phase of Mars landing, and current results can be primarily classified into two categories: in the first category, optimization or other methods are used to generate an optimal trajectory, and in the second category, the lander is guided to track the desired trajectory which is determined by offline optimization. The desired trajectory may be chosen based on the previous experience or a solution of a constrained optimization problem. For the trajectory optimization, Blackmore et al. proposed a Mars landing trajectory with minimum terminal errors using a convex optimization method [5]. Acikmese et al. focused on the fuel optimality and designed a guidance scheme subject to certain constraints [2]. Although the trajectory optimization methods have many advantages, they cannot be applied on-board easily due to its large computational burden. For the tracking guidance approach, tracking control methods are usually employed to track the trajectory pre-defined in the first phase. Tu et al. proposed a drag-based tracking guidance scheme for Mars precision landing missions, which was proven useful in enhancing tracking accuracy due to its prediction ability [21]. Liang et al. proposed a robust tracking guidance scheme for pinpoint soft landing missions, which can guarantee the landing precision subject to uncertainty and disturbances [18]. Compared with the trajectory optimization methods, tracking guidance approaches have less computational burden, and their fuel consumptions depend on the nominal trajectories and the environment. The robustness and the convergence rate cannot be guaranteed. Compared with landing on airless planets [24], [7], one of the biggest challenge of Mars landing is the complex atmosphere, which introduces unknown disturbances. So for precision landing missions, the Martian atmosphere should be fully considered. Therefore, for the next generation Mars landing missions, it is important to design an autonomous and robust landing guidance scheme for the powered descent phase.

The existing literatures on the autonomous Mars landing guidance design problem are as follows. Huang et al. designed an autonomous optimal guidance for asteroids landing missions, which ensured the soft landing with small landing errors [14]. Gaskell et al. proposed an imaging data based guidance to achieve autonomous landing on small planets, which was effective during powered descent phase [10]. Guo et al. proposed a zero-effort-miss/zero-effort-velocity (ZEM/ZEV) optimal feedback guidance for Mars powered descent phase, which ensured the fuel optimality [12]. Yao et al. proposed an improved ZEM/ZEV guidance by adding a collision avoidance term, which was proven effective to cope with the hazard avoidance problem [25]. Guo et al. designed a waypoint method based ZEM/ZEV guidance to simplify the optimal solution during the landing process [13]. However, all these methods cannot effectively cope with unknown disturbances. The disturbances are mainly caused by dust storms and model uncertianties during the powered descent phase [3]. The dust storms generally appear suddenly [11] at an average speed

This work is sponsored by the National Natural Science Foundation of China (Grant Nos. 61174200, 61304005, 61403103)

Y. Zhang is a postdoctoral researcher with Queen Mary University of London, UK, E1 4NS. e-mail: yao.zhang@qmul.ac.uk.

R. Vepa is with Queen Mary University of London, UK, E1 4NS. e-mail: r.vepa@qmul.ac.uk.

G. Li, the corresponding author, is with Queen Mary University of London, UK, E1 4NS. e-mail: g.li@qmul.ac.uk.

T. Zeng is with Beijing Institute of Technology, China, 100081. e-mail: tianyi.zeng@qmul.ac.uk.

Manuscript received.....

of 27m/s [15]. In this paper, we consider all the unknown disturbances including atmospheric dispersions, knowledge errors and Martian wind by lumping them into one acceleration disturbance term.

Due to the clear physical significance and the strong robustness, the multiple sliding surfaces (MSS) technique is attractive for many space applications [17], [22]. MSS has already attracted some attention in the autonomous precision landing guidance field. Furfaro et al. developed a multiple sliding surfaces guidance for asteroid landing missions, which was robust against disturbances [8], while the convergence speed can be further improved. Furfaro et al. proposed a terminal multiple surface guidance for planetary landing, which employed a reinforcement learning method to guarantee optimality [9], while the guidance performance relies on the initial states. Although the guidance schemes in these papers are finite-time stable, the maximum convergence time is mainly based on the initial state, which reduces the reliability to some extent. Not all the upper bounds of sliding surfaces convergence time can be exactly known because of the measurement errors of the initial states. When the actual convergence time of one of the sliding surfaces is larger than the pre-determined whole flight time, the guidance fails to lead the lander to the target landing site with zero velocity. To cope with this problem, the fixed time stabilization technique is employed in this paper to ensure that all the sliding surfaces can converge to zero within a pre-defined time, which is independent on the initial state. Once the parameters of the proposed guidance are fixed, we can obtain the maximum convergence time and maximum landing error with any initial positions and velocities.

This paper proposes an autonomous and robust guidance scheme for the precision Mars landing missions. The proposed guidance is mainly based on a recent development in control theory, which is the fixed-time stabilization method. The main advantages of the proposed guidance include 1) it can ensure the lander to achieve a precision landing within a pre-defined fixed time with or without measurement errors and unknown disturbances; 2) compared with offline fuel optimal guidance, the collisions can be avoided subject to the disturbance with acceptable fuel assumption; 3) compared with the super-twisting sliding-mode guidance, it consumes less fuel and maintains faster convergence speed. Furthermore, since convergence exactly at the equilibrium point leads to a conservative estimation of the convergence time and this is not necessary in some cases, this paper proposes a practical fixed-time stabilization theorem and conducts the robustness analysis for the proposed guidance scheme. In addition, the parameters of the proposed guidance can be tuned according to the demand of the landing time in practical missions. So once the desired landing time is set, we can determine the parameters of the proposed guidance to ensure that the whole landing time does not exceed the desired time irrespective of lander's initial position and initial velocity.

II. Practical Fixed-time Stabilization Technique

In this section, the finite-time stabilization technique and the fixed-time stabilization technique are introduced as a foundation of the proposed method.

A. Finite-time stabilization and fixed-time stabilization

Finite-time stabilization theory was proposed in [4], and its definition and Lyapunov theorem are stated below for completeness.

Lemma 1. *(Finite-time stabilization). For the system (1),*

$$\dot{x}(t) = f(x(t)) \tag{1}$$

the equilibrium point $x = 0$ of the system is finite-time stable, if there exists a Lyapunov function $V_a : \mathbb{U} \to \mathbb{R}$ satisfying two conditions: 1) $V_a \geq 0$; 2) $\dot{V}_a(x) \leq -\alpha V_a^p(x), x \in \mathbb{U}_0$, where $\alpha > 0$, $0 < p < 1$ and $\mathbb{U}_0 \subset \mathbb{U}$. The convergence time is $T_a \leq \frac{V_0^{1-p}}{\alpha(1-p)}$. Here $x \in \mathbb{R}^n$, $\mathbb{U} \subset \mathbb{R}^n$ and $f : \mathbb{U}_0 \to \mathbb{R}^n$ is continuous in an open neighborhood $\mathbb{U}_0$ of the origin.

Fixed-time stabilization theory is an improved finite-time method by adding another exponential term in the Lyapunov function [19], and the main advantage of using the fixed-time stabilization theorey is that it can drive the system state to the equilibrium point within a pre-defined time.

Definition 1. *(Fixed-time stabilization). The equilibrium point $x = 0$ of the system (1) is fixed time stable if it is globally finite-time stable (FTS) and the convergence time T_b from any initial state to equilibrium point is bounded, i.e. there exists a positive constant T_{bMAX} such that $T_b(x) \leq T_{bMAX}$ can be established for any $x \in \mathbb{R}^n$.*

Lemma 2. *(Lyapunov function of fixed-time stabilization). Consider the system (1). Suppose that there is a Lyapunov function V_b defined on the neighborhood $\mathbb{U} \subset \mathbb{R}^n$ of the origin, and condition*

$$\dot{V}_b(x) \leq -(\alpha V_b(x)^p + \beta V_b(x)^g)^k \tag{2}$$

can be satisfied. Then the origin of the system (1) is fixed-time stable, and any $V(x)$ can reach $V(x) \equiv 0$ in a fixed time of T_b, which is bounded and its bound is independent on the initial states:

$$T_b \leq \frac{1}{\alpha^k(1-pk)} + \frac{1}{\beta^k(gk-1)} \tag{3}$$

where $\alpha, \beta, p, k \in R^+$, $pk < 1$ and $gk > 1$.

It can be seen that the upper bound of convergence time can be obtained without any knowledge of $V_b(x_0)$, and this is the primary advantage of the fixed-time stabilization over the finite-time stabilization.

Driving the system state to the exactly equilibrium point is rather difficult when the disturbance caused by the model uncertainty and the extra interference are considered. Thus, it is necessary to investigate the practical fixed-time stabilization technique.

B. Practical fixed-time stabilization

Practical fixed-time stabilization technique can drive the system state within a neighborhood of the origin when disturbances and model uncertainties are considered.

Theorem 1. *Consider the system (1). Suppose that there is a Lyapunov function $V_c(x)$ defined on the neighborhood $\mathbb{U} \subset \mathbb{R}^n$ of the origin, and*

$$\dot{V}_c(x) \leq -(\alpha V_c(x)^p + \beta V_c(x)^g)^k + \eta \tag{4}$$

is satisfied, then the origin of the system (1) is fixed-time stable, and any $V_c(x)$ can reach within the neighborhood

$$\{\lim_{t\to T_c} x | V_c(x) \leq \min\{(\frac{\eta}{\alpha^k(1-\theta^k)})^{\frac{1}{pk}}, (\frac{\eta}{\beta^k(1-\theta^k)})^{\frac{1}{gk}}\}\} \tag{5}$$

in a fixed time expressed by T_c, which is bounded and its bound is independent on the initial states:

$$T_c \leq \frac{1}{\alpha^k\theta^k(1-pk)} + \frac{1}{\beta^k\theta^k(gk-1)} \tag{6}$$

where $0 < \theta < 1$, $\alpha, \beta, p, k \in R^+$, $\eta > 0$, $pk < 1$ and $gk > 1$.

Proof. There exists a scalar $0 < \theta < 1$ such that the Lyapunov function (4) can be rewritten as

$$\begin{aligned} \dot{V}_c(x) \leq & -(1-\theta^k)((\alpha V_c(x)^p + \beta V_c(x)^g)^k) \\ & -\theta^k((\alpha V_c(x)^p + \beta V_c(x)^g)^k) + \eta \end{aligned} \tag{7}$$

Clearly, $\dot{V}_c(x) \leq -\theta^k((\alpha V_c(x)^p + \beta V_c(x)^g)^k)$ is established if the condition (8) is satisfied.

$$-(1-\theta^k)((\alpha V_c(\boldsymbol{x})^p + \beta V_c(\boldsymbol{x})^g)^k) + \eta \leq 0 \tag{8}$$

Therefore, the neighborhood of the origin is

$$(\alpha V_c(x)^p + \beta V_c(x)^g)^k \geq \frac{\eta}{1-\theta^k} \tag{9}$$

It is obvious that $\dot{V}_c(x) < 0$, if $V_c(x)$ is outside the neighborhood (5). This means that $V_c(x)$ can keep converging to the origin and stable within the neighborhood eventually. The convergence time (6) can be calculated by employing *Lemma* 2. □

III. Practical Fixed-time Stabilization Technique Based Mars Landing Guidance Design

In this section, the mathematical model of the lander during powered descent phase is introduced firstly. Secondly, the guidance based on fixed-time stabilization technique is proposed, which can address the disturbance problem and ensure the lander to achieve a precision landing within a fixed time. The practical fixed-time stabilization technique is used in the proposed guidance.

A. Mathematical model of the lander

A non-rotating inertial coordinate frame fixed on the Martian surface is established, where the target landing site is the origin and the three axes are crossrange, downrange and altitude, as shown in Figure 1. At the beginning of the powered descent phase, the relative distance between the lander and the Martian surface is 2000–5000m, and the relative velocity is within 1000m/s. The model of the lander during powered descent phase can be expressed as:

$$\dot{\boldsymbol{r}} = \boldsymbol{v} \tag{10}$$

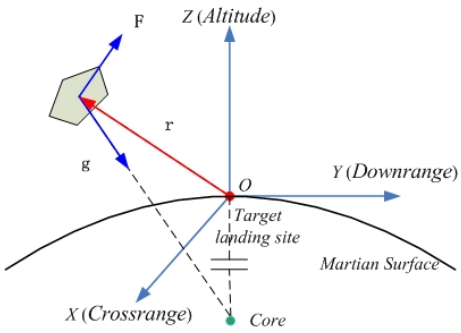

Fig. 1. Surface fixed coordinate frame

$$\dot{\boldsymbol{v}} = \boldsymbol{a} + \boldsymbol{g} + \boldsymbol{a_m} \tag{11}$$

where $\boldsymbol{r} = \begin{bmatrix} r_x & r_y & r_z \end{bmatrix}^{\mathrm{T}}$ is the position vector, $\boldsymbol{v} = \begin{bmatrix} v_x & r_y & r_z \end{bmatrix}^{\mathrm{T}}$ is the velocity vector, $\boldsymbol{g} = \begin{bmatrix} 0 & 0 & g \end{bmatrix}^{\mathrm{T}}$ is the Martian gravitational acceleration, and $\boldsymbol{a} = \begin{bmatrix} a_x & a_y & a_z \end{bmatrix}^{\mathrm{T}}$ is the command acceleration provided by thrusters, $\boldsymbol{a_m} = \begin{bmatrix} a_{mx} & a_{my} & a_{mz} \end{bmatrix}^{\mathrm{T}}$ denotes the Martian atmosphere disturbance acceleration and its model [6] is approximated by

$$a_{mi} = -0.699 v_i^2 e^{-0.0009 r_z}/A_i m, i = x, y, z \tag{12}$$

where r_z denotes the altitude of the lander relative to the Martian surface, and $A_i, i = x, y, z$ are the effective cross-sectional area perpendicular to x-axis, y-axis and z-axis, respectively, $v_i, i = x, y, z$ is the velocity of the lander, and m is the mass of the lander.

Note that the lander mass variation should be considered to obtain the precision model by employing a classical rocket equation as follows.

$$\dot{m} = -\frac{\|\boldsymbol{F}\|}{c} \tag{13}$$

$$\boldsymbol{a} = \frac{\boldsymbol{F}}{m} \tag{14}$$

where m is the lander mass, $\boldsymbol{F} = \begin{bmatrix} F_x & F_y & F_z \end{bmatrix}^{\mathrm{T}}$ is the thruster force and its magnitude is expressed as $\|\boldsymbol{F}\| = \sqrt{F_x^2 + F_y^2 + F_z^2}$ and $c = I_{sp} g_e$ is a constant, where I_{sp} is the thrusters impulse and g_e is the gravitational acceleration at sea level.

B. Fixed-time stabilization technique based guidance design

For a practical Mars landing scenario, there exists an upper bound of mission time (i.e. flight time) expressed by t_f, which leads to the requirement of the fast convergence speed. Thus, the convergence time should be limited within this upper bound.

In this paper, two sliding surfaces and two sliding-mode reaching laws are designed. The relation between them is that the second sliding surface is derived from the first sliding mode reaching law, which enables the system state to satisfy the first sliding mode reaching law automatically after arriving at the second sliding surface.

Define the first sliding surface as the position of the lander:

$$\boldsymbol{s}_1 = \boldsymbol{r} - \boldsymbol{r}_d \tag{15}$$

where $\boldsymbol{r} \in \mathbb{R}^3$ is the position vector of the lander and $\boldsymbol{r}_d \in R^3$ is the desired position vector. $\boldsymbol{s}_1 = \begin{bmatrix} s_{1x} & s_{1y} & s_{1z} \end{bmatrix}$, where s_{1x}, s_{1y} and s_{1z} denote the crossrange, downrange and altitude direction component of the position tracking error, respectively.

Design the first reaching law as

$$\dot{\boldsymbol{s}}_1 = -\boldsymbol{\beta}_1 |\boldsymbol{s}_1|^{q_1} \mathrm{sgn}(\boldsymbol{s}_1) - \boldsymbol{\beta}_2 |\boldsymbol{s}_1|^{q_2} \mathrm{sgn}(\boldsymbol{s}_1) \tag{16}$$

where $\boldsymbol{\beta}_1 = \mathrm{diag}\{\beta_{1x}, \beta_{1y}, \beta_{1z}\}$ and $\boldsymbol{\beta}_2 = \mathrm{diag}\{\beta_{2x}, \beta_{2y}, \beta_{2z}\}$ are diagonal constant matrices. q_1 and q_2 are constants, where $\beta_{1i} > 0, \beta_{2i} > 0, 0 < q_1 < 1, q_2 > 1$ with $i = x, y, z$. The sign function $\mathrm{sgn}(\cdot)$ is

$$\mathrm{sgn}(\Delta) = \begin{cases} 1 & \Delta > 0 \\ 0 & \Delta = 0 \\ -1 & \Delta < 0 \end{cases} \tag{17}$$

Theorem 2. *For the system (11), the sliding surface (15) and its time derivative can be driven to zero in a finite time for any initial states under the sliding-mode reaching law (16), and the upper bound of the convergence time is*

$$\boldsymbol{T}_1 \leq \frac{1}{\boldsymbol{\beta}_1 (1 - q_1) 2^{\frac{q_1 - 1}{2}}} + \frac{1}{\boldsymbol{\beta}_2 (q_2 - 1) 2^{\frac{q_2 - 1}{2}}} \tag{18}$$

Proof. Choose a Lyapunov function

$$\boldsymbol{V}_1 = \frac{1}{2} \boldsymbol{s}_1^{\mathrm{T}} \boldsymbol{s}_1 > 0 \tag{19}$$

Then, its time derivative is

$$\begin{aligned} \dot{\boldsymbol{V}}_1 &= \boldsymbol{s}_1^{\mathrm{T}} \dot{\boldsymbol{s}}_1 \\ &= \boldsymbol{s}_1^{\mathrm{T}} (-\boldsymbol{\beta}_1 |\boldsymbol{s}_1|^{q_1} \mathrm{sgn}(\boldsymbol{s}_1) - \boldsymbol{\beta}_2 |\boldsymbol{s}_1|^{q_2} \mathrm{sgn}(\boldsymbol{s}_1)) \\ &= -\boldsymbol{\beta}_1 |\boldsymbol{s}_1|^{q_1 + 1} - \boldsymbol{\beta}_2 |\boldsymbol{s}_1|^{q_2 + 1} \\ &\leq -(\boldsymbol{\beta}_1 2^{\frac{q_1 + 1}{2}} \boldsymbol{V}_1^{\frac{q_1 + 1}{2}} + \boldsymbol{\beta}_2 2^{\frac{q_2 + 1}{2}} \boldsymbol{V}_1^{\frac{q_2 + 1}{2}}) \end{aligned} \tag{20}$$

It is obvious that this Lyapunov function satisfies the conditions of $Lemma$ 2. □

From $Theorem$ 2, it can be found that once the first sliding surface and its derivative satisfy the designed first reaching law (16), the system state converges to the equilibrium point $\dot{\boldsymbol{s}} = \boldsymbol{s} = 0$ within a fixed time, that is, any initial position and velocity of the lander can be driven to zero in a fixed time if (16) is established.

However, this reaching law cannot be guaranteed in all cases, because even though we initially set the correlation between system states $\boldsymbol{s}$ and $\dot{\boldsymbol{s}}$ as (16), there are disturbances, model uncertainties and measuring errors. Thus, it is necessary to design another sliding mode to steer system states, no matter where they are, to the first sliding mode in a fixed time.

The second sliding surface design employes the MSSG method to make the equilibrium point of the second sliding surface equal to the correlation expressed in (16). When the second sliding surface converges to zero, the first sliding mode reaching law is established automatically, which then drives the system state to its equilibrium point.

The second sliding surface is designed as

$$\boldsymbol{s}_2 = \dot{\boldsymbol{s}}_1 + \boldsymbol{\beta}_1 |\boldsymbol{s}_1|^{q_1} \mathrm{sgn}(\boldsymbol{s}_1) + \boldsymbol{\beta}_2 |\boldsymbol{s}_1|^{q_2} \mathrm{sgn}(\boldsymbol{s}_1) \tag{21}$$

Its derivative is

$$\dot{\boldsymbol{s}}_2 = \ddot{\boldsymbol{s}}_1 + \boldsymbol{\beta}_1 q_1 |\boldsymbol{s}_1|^{q_1 - 1} \dot{\boldsymbol{s}}_1 + \boldsymbol{\beta}_2 q_2 |\boldsymbol{s}_1|^{q_2 - 1} \dot{\boldsymbol{s}}_1 \tag{22}$$

Considering that $\ddot{\boldsymbol{s}}_1 = \ddot{\boldsymbol{r}} - \ddot{\boldsymbol{r}}_d = \dot{\boldsymbol{v}} - \dot{\boldsymbol{v}}_d$ and $\boldsymbol{v}_d = 0$ due to the soft landing requirment, we have

$$\ddot{\boldsymbol{s}}_1 = \dot{\boldsymbol{v}} = \boldsymbol{a} + \boldsymbol{g} + \boldsymbol{a}_m \tag{23}$$

By substituting (23) into (22), the command acceleration explicitly appears in the equation of the second sliding surface as follows:

$$\begin{aligned} \dot{\boldsymbol{s}}_2 =& \dot{\boldsymbol{v}} \\ =& \boldsymbol{a} + \boldsymbol{g} + \boldsymbol{a}_m \\ & - \boldsymbol{\beta}_1^2 q_1 |\boldsymbol{s}_1|^{2q_1 - 1} \mathrm{sgn}(\boldsymbol{s}_1) - \boldsymbol{\beta}_2^2 q_2 |\boldsymbol{s}_1|^{2q_2 - 1} \mathrm{sgn}(\boldsymbol{s}_1) \\ & - \boldsymbol{\beta}_1 \boldsymbol{\beta}_2 (q_1 + q_2) |\boldsymbol{s}_1|^{q_1 + q_2 - 1} \mathrm{sgn}(\boldsymbol{s}_1) \end{aligned} \tag{24}$$

Theorem 3. *For the system (21), the system state $\boldsymbol{s}_2$ converges to zero within a fixed time under the proposed guidance*

$$\begin{aligned} \boldsymbol{a} =& -\boldsymbol{g} - \boldsymbol{a}_m + \boldsymbol{\beta}_1^2 q_1 |\boldsymbol{s}_1|^{2q_1 - 1} \mathrm{sgn}(\boldsymbol{s}_1) + \boldsymbol{\beta}_2^2 q_2 |\boldsymbol{s}_1|^{2q_2 - 1} \mathrm{sgn}(\boldsymbol{s}_1) \\ & + \boldsymbol{\beta}_1 \boldsymbol{\beta}_2 (q_1 + q_2) |\boldsymbol{s}_1|^{q_1 + q_2 - 1} \mathrm{sgn}(\boldsymbol{s}_1) \\ & - \boldsymbol{\alpha}_1 |\boldsymbol{s}_2|^{g_1} \mathrm{sgn}(\boldsymbol{s}_2) - \boldsymbol{\alpha}_2 |\boldsymbol{s}_2|^{g_2} \mathrm{sgn}(\boldsymbol{s}_2) \end{aligned} \tag{25}$$

where $\boldsymbol{\alpha}_1 = \mathrm{diag}\{\alpha_{1x}, \alpha_{1y}, \alpha_{1z}\}$ and $\boldsymbol{\alpha}_2 = \mathrm{diag}\{\alpha_{2x}, \alpha_{1y}, \alpha_{2z}\}$ are diagonal constant matrices, where $\alpha_{1i} > 0$, $\alpha_{2i} > 0$, with $i = x, y, z$. $0 < g_1 < 1$ and $g_2 > 1$ are constants. The upper bound of the convergence time is

$$\boldsymbol{T}_2 \leq \frac{1}{\boldsymbol{\alpha}_1 (1 - g_1) 2^{\frac{g_1 - 1}{2}}} + \frac{1}{\boldsymbol{\alpha}_2 (g_2 - 1) 2^{\frac{g_2 - 1}{2}}}, \tag{26}$$

which is independent on the initial state.

Proof. Design the following Lyapunov function

$$\boldsymbol{V}_2 = \frac{1}{2} \boldsymbol{s}_2^{\mathrm{T}} \boldsymbol{s}_2 \tag{27}$$

which is nonnegative and its time derivative is

$$\begin{aligned} \dot{\boldsymbol{V}}_2 =& \boldsymbol{s}_2^{\mathrm{T}} \dot{\boldsymbol{s}}_2 \\ =& \boldsymbol{s}_2^{\mathrm{T}} [\boldsymbol{a} + \boldsymbol{g} + \boldsymbol{a}_m - \boldsymbol{\beta}_1^2 q_1 |\boldsymbol{s}_1|^{2q_1 - 1} \mathrm{sgn}(\boldsymbol{s}_1) \\ & - \boldsymbol{\beta}_2^2 q_2 |\boldsymbol{s}_1|^{2q_2 - 1} \mathrm{sgn}(\boldsymbol{s}_1) \\ & - \boldsymbol{\beta}_1 \boldsymbol{\beta}_2 (q_1 + q_2) |\boldsymbol{s}_1|^{q_1 + q_2 - 1} \mathrm{sgn}(\boldsymbol{s}_1)] \end{aligned} \tag{28}$$

Substituting the proposed guidance (25) into (28) gives

$$\begin{aligned} \dot{\boldsymbol{V}}_2 =& \boldsymbol{s}_2^{\mathrm{T}} [-\boldsymbol{\alpha}_1 |\boldsymbol{s}_2|^{g_1} \mathrm{sgn}(\boldsymbol{s}_2) - \boldsymbol{\alpha}_2 |\boldsymbol{s}_2|^{g_2} \mathrm{sgn}(\boldsymbol{s}_2)] \\ \leq & -\boldsymbol{\alpha}_1 |\boldsymbol{s}_2|^{g_1 + 1} - \boldsymbol{\alpha}_2 |\boldsymbol{s}_2|^{g_2 + 1} \\ \leq & -(\boldsymbol{\alpha}_1 2^{\frac{g_1 + 1}{2}} \boldsymbol{V}_2^{\frac{g_1 + 1}{2}} + \boldsymbol{\alpha}_2 2^{\frac{g_2 + 1}{2}} \boldsymbol{V}_2^{\frac{g_2 + 1}{2}}) \end{aligned} \tag{29}$$

It is clear that this Lyapunov function can satisfy the conditions of $Lemma$ 2. □

From the proposed $Theorem$ 2 and $Theorem$ 3, we find that the upper bounds of the convergence time $\boldsymbol{T}_1$ and $\boldsymbol{T}_2$ do not involve any information of the initial states, so that the states can be driven to the equilibrium point within a predefined time independent on the initial states. This property

has a practical significance in the powered descent phase guidance design for the Mars lander. This is because during the parachute phase, the preceding stage, the lander is not controlled, which may lead to a large initial error of powered descent phase. The proposed guidance can ensure the lander to achieve a precision landing in a finite time in all cases, and the upper bound of the convergence time can be calculated in advance according to parameters of the proposed guidance. The parameters of the proposed guidance can be tuned according to a specific upper bound of the convergence time t_f as follows: $\max\{\frac{1}{\beta_{1i}(1-q_1)2^{\frac{q_1-1}{2}}}+\frac{1}{\beta_{2i}(q_2-1)2^{\frac{q_2-1}{2}}}\}\leq t_f$ and $\max\{\frac{1}{\alpha_{1i}(1-g_1)2^{\frac{g_1-1}{2}}}+\frac{1}{\alpha_{2i}(g_2-1)2^{\frac{g_2-1}{2}}}\}\leq t_f$ where $i=x,y,z$.

Remark 1. For the lander equipped with thrust-limited engines, it is important to provide the minimum value of t_f for a soft landing. The terminal position and velocity constraints are $r_f=0$ and $v_f=0$, and we assume the maximum acceleration provided by thrusters is a_{max}. Then, we can respectively obtain the minimum values of t_f to ensure the position and velocity to converge to zero. For the position to converge to zero with a minimum time, it can be calculated by $t_{f1i}=\frac{-v_{0i}+(v_{0i}^2-2a_{max}r_{0i})^{\frac{1}{2}}}{a_{max}}$, where r_{0i} and v_{0i} denote the initial position and velocity of the lander along $i-$axis, $i=x,y,z$. For the velocity to converge to zero with a minimum time, it can be calculated by $t_{f2i}=\frac{-v_{0i}}{a_{max}-g_i}$. Therefore, we can give the lower bound of the t_f, which is $t_f\geq\max\{t_{f1i},t_{f2i}\}$. The upper bound of the t_f is usually set as a maximum landing time, which depends on the requirement of a specific mission.

Remark 2. Each parameter has its own effect on the performance of the proposed guidance. The parameters $\boldsymbol{\alpha}_1$, $\boldsymbol{\alpha}_2$, $\boldsymbol{\beta}_1$ and $\boldsymbol{\beta}_2$ denote the gain coefficient matrices, and their diagonal elements should be set as positive constants. Large values of these parameters accelerate the whole landing process; however, if the values are too large, the control input may exceed the thrust limitation of an engine. The coefficients q_1, q_2, p_1 and p_2 are designed to satisfy the conditions of $Theorem$ 2. q_1 and p_1 are chosen between 0 and 1, and q_2 and p_2 are set greater than 1. The convergence time is reduced if the values of $1-q_1$, $1-p_1$, q_2-1 and p_2-1 are large. But the peak value of the thrust is increased. Considering that the lander is equipped with thrust-limited engines in practical missions, we can decrease the values of $1-q_1$, $1-p_1$, q_2-1 and p_2-1 to reduce the control input. Therefore, it is recommended that under the conditions of (30) and (31), the values of $1-q_1$, $1-p_1$, q_2-1 and p_2-1 are set as small as possible.

C. Robustness analysis based on practical fixed-time stabilization technique

Taking the disturbance caused by gusty wind and model uncertainty into account, we investigate the robustness of the proposed guidance using the proposed practical fixed-time stabilization theorem ($Theorem$ 1), and a new convergence time and the neighborhood of the origin are given in this section. The proposed guidance (25) can drive the lander into the neighborhood of the target landing site in a fixed time when the disturbance with known upper bound a_{pMAX} is known.

The new dynamic model of the lander is

$$\dot{\boldsymbol{v}}=\boldsymbol{a}+\boldsymbol{g}+\boldsymbol{a}_m+\boldsymbol{a}_p \tag{30}$$

where $\boldsymbol{a}_p$ is the equivalent disturbance acceleration.

Hypothesis 1. *The disturbance acceleration $\boldsymbol{a}_p$ is bounded, and its upper bound a_{pMAX} is known, which is strictly positive, i.e. there always exists a positive constant a_{pMAX} satisfying $\|\boldsymbol{a}_p\|\leq a_{pMAX}$.*

Theorem 4. *For the system (30), the proposed guidance (25) can ensure the terminal position of the lander to land within a neighborhood area of the target landing site in a fixed time, and the neighborhood and the upper bound of the convergence time are expressed in (31) and (32).*

$$|r_i|\leq\min\{(\frac{M_i}{(1-\theta_2)\beta_{1i}})^{\frac{1}{q_1}},(\frac{M_i}{(1-\theta_2)\beta_{2i}})^{\frac{1}{q_2}}\} \tag{31}$$

where $M_i=\min\{(\frac{a_{pMAX}}{(1-\theta_1)\alpha_{1i}})^{\frac{1}{g_1}},(\frac{a_{pMAX}}{(1-\theta_1)\alpha_{2i}})^{\frac{1}{g_2}}\}$, $i=x,y,z$, *and* $0<\theta_1,\theta_2<1$ *are constants.*

$$\begin{aligned}T_{3i}\leq\max\{&\frac{1}{\alpha_{1i}\theta_1(1-g_1)2^{\frac{g_1-1}{2}}}+\frac{1}{\alpha_{2i}\theta_1(g_2-1)2^{\frac{g_2-1}{2}}},\\&\frac{1}{\beta_{1i}\theta_2(1-q_1)2^{\frac{q_1-1}{2}}}+\frac{1}{\beta_{2i}\theta_2(q_2-1)2^{\frac{q_2-1}{2}}}\}\end{aligned} \tag{32}$$

Proof. For the system (30), (23) can be rewritten as

$$\ddot{\boldsymbol{s}}_1=\dot{\boldsymbol{v}}=\boldsymbol{a}+\boldsymbol{g}+\boldsymbol{a}_m+\boldsymbol{a}_p \tag{33}$$

and the derivative of the second sliding surface is

$$\begin{aligned}\dot{\boldsymbol{s}}_2=&\boldsymbol{a}+\boldsymbol{g}+\boldsymbol{a}_m+\boldsymbol{a}_p\\&-\boldsymbol{\beta}_1^2q_1|\boldsymbol{s}_1|^{2q_1-1}\mathrm{sgn}(\boldsymbol{s}_1)-\boldsymbol{\beta}_2^2q_2|\boldsymbol{s}_1|^{2q_2-1}\mathrm{sgn}(\boldsymbol{s}_1)\\&-\boldsymbol{\beta}_1\boldsymbol{\beta}_2(q_1+q_2)|\boldsymbol{s}_1|^{q_1+q_2-1}\mathrm{sgn}(\boldsymbol{s}_1)\end{aligned} \tag{34}$$

Then, for the Lyapunov function (27), its time derivative is

$$\begin{aligned}\dot{\boldsymbol{V}}_2=&\boldsymbol{s}_2^{\mathrm{T}}\dot{\boldsymbol{s}}_2\\=&\boldsymbol{s}_2^{\mathrm{T}}[\boldsymbol{a}+\boldsymbol{g}+\boldsymbol{a}_m+\boldsymbol{a}_p\\&-\boldsymbol{\beta}_1^2q_1|\boldsymbol{s}_1|^{2q_1-1}\mathrm{sgn}(\boldsymbol{s}_1)-\boldsymbol{\beta}_2^2q_2|\boldsymbol{s}_1|^{2q_2-1}\mathrm{sgn}(\boldsymbol{s}_1)\\&-\boldsymbol{\beta}_1\boldsymbol{\beta}_2(q_1+q_2)|\boldsymbol{s}_1|^{q_1+q_2-1}\mathrm{sgn}(\boldsymbol{s}_1)]\end{aligned} \tag{35}$$

Substituting the proposed guidance (25) into (35) gives

$$\begin{aligned}\dot{\boldsymbol{V}}_2=&\boldsymbol{s}_2^{\mathrm{T}}[-\boldsymbol{a}_p-\boldsymbol{\alpha}_1|\boldsymbol{s}_2|^{g_1}\mathrm{sgn}(\boldsymbol{s}_2)-\boldsymbol{\alpha}_2|\boldsymbol{s}_2|^{g_2}\mathrm{sgn}(\boldsymbol{s}_2)]\\\leq&-\boldsymbol{\alpha}_1|\boldsymbol{s}_2|^{g_1+1}-\boldsymbol{\alpha}_2|\boldsymbol{s}_2|^{g_2+1}+a_{pMAX}|\boldsymbol{s}_2|\\\leq&-(\boldsymbol{\alpha}_12^{\frac{g_1+1}{2}}\boldsymbol{V}_2^{\frac{g_1+1}{2}}+\boldsymbol{\alpha}_22^{\frac{g_2+1}{2}}\boldsymbol{V}_2^{\frac{g_2+1}{2}})+a_{pMAX}|\boldsymbol{s}_2|\end{aligned} \tag{36}$$

By employing $Theorem$ 1, we can establish (37):

$$\begin{aligned}\frac{1}{2}s_{2x}^2\leq\min\{&(\frac{a_{pMAX}|s_{2x}|}{\alpha_{1x}2^{\frac{g_1+1}{2}}(1-\theta_1)})^{\frac{2}{g_1+1}},\\&(\frac{a_{pMAX}|s_{2x}|}{\alpha_{2x}2^{\frac{g_2+1}{2}}(1-\theta_1)})^{\frac{2}{g_2+1}}\}\end{aligned} \tag{37}$$

For the expression convenience, we only give the derivation of the x-axis component, and the derivations of the other two axes components are similar to it.

From (37), it can be found that the neighborhood of the origin $s_{2x}=0$ is

$$|s_{2x}| \leq \min\{(\frac{a_{pMAX}}{(1-\theta_1)\alpha_{1x}})^{\frac{1}{g_1}}, (\frac{a_{pMAX}}{(1-\theta_1)\alpha_{2x}})^{\frac{1}{g_2}}\} \quad (38)$$

Similarly, three components of the system state $\boldsymbol{s}_2$ satisfies

$$|s_{2i}| \leq \min\{(\frac{a_{pMAX}}{(1-\theta_1)\alpha_{1i}})^{\frac{1}{g_1}}, (\frac{a_{pMAX}}{(1-\theta_1)\alpha_{2i}})^{\frac{1}{g_2}}\}, \quad (39)$$

and the convergence time is expressed as

$$T_{2i} \leq \frac{1}{\alpha_{1i}\theta_1(1-g_1)2^{\frac{g_1-1}{2}}} + \frac{1}{\alpha_{2i}\theta_1(g_2-1)2^{\frac{g_2-1}{2}}} \quad (40)$$

(39) provides a neighborhood of $\boldsymbol{s}_2$, and to explicitly express the neighborhood of the position and velocity of the lander, it is necessary to give the neighborhood of $\boldsymbol{s}_1$ and its derivative. Define $M_i = \min\{(\frac{a_{pMAX}}{(1-\theta_1)\alpha_{1i}})^{\frac{1}{g_1}}, (\frac{a_{pMAX}}{(1-\theta_1)\alpha_{2i}})^{\frac{1}{g_2}}\}$, with $M_i > 0$. From (21), the i-axis component of the first reaching law is

$$\dot{s}_{1i} = -\beta_{1i}|s_{1i}|^{q_1}\mathrm{sgn}(s_{1i}) - \beta_{2i}|s_{1i}|^{q_2}\mathrm{sgn}(s_{1i}) + s_{2i} \quad (41)$$

For the Lyapunov function (19), the time derivative of its i-axis component is

$$\begin{aligned}\dot{V}_{1i} &= s_{1i}\dot{s}_{1i} \\ &= -\beta_{1i}|s_{1i}|^{q_1+1} - \beta_{2i}|s_{1i}|^{q_2+1} + s_{1i}s_{2i} \\ &\leq -\beta_{1i}|s_{1i}|^{q_1+1} - \beta_{2i}|s_{1i}|^{q_2+1} + M_i|s_{1i}| \\ &\leq -\beta_{1i}2^{\frac{q_1+1}{2}}V_{1i}^{\frac{q_1+1}{2}} - \beta_{2i}2^{\frac{q_2+1}{2}}V_{1i}^{\frac{q_2+1}{2}} + M_i|s_{1i}|\end{aligned} \quad (42)$$

We obtain (43) below by utilizing $Theorem$ 1:

$$\begin{aligned}\frac{1}{2}s_{1i}^2 \leq \min\{&(\frac{M_i|s_{1i}|}{\beta_{1i}2^{\frac{q_1+1}{2}}(1-\theta_2)})^{\frac{2}{q_1+1}}, \\ &(\frac{M_i|s_{1i}|}{\beta_{2i}2^{\frac{q_2+1}{2}}(1-\theta_2)})^{\frac{2}{q_2+1}}\}\end{aligned} \quad (43)$$

Therefore, the neighborhood of the origin $\boldsymbol{s}_1 = 0$ is

$$|s_{1i}| \leq \min\{(\frac{M_i}{(1-\theta_2)\beta_{1i}})^{\frac{1}{q_1}}, (\frac{M_i}{(1-\theta_2)\beta_{2i}})^{\frac{1}{q_2}}\} \quad (44)$$

The convergence time is

$$T_{1i} \leq \frac{1}{\beta_{1i}\theta_2(1-q_1)2^{\frac{q_1-1}{2}}} + \frac{1}{\beta_{2i}\theta_2(q_2-1)2^{\frac{q_2-1}{2}}} \quad (45)$$

Thus, the upper bound of the convergence time is $T_{3i} = \max\{T_{1i}, T_{2i}\}$. □

It can be seen from (32) that compared with the guidance based on the fixed-time stabilization technique, the practical fixed-time stabilization technique based guidance has a larger upper bound of the convergence time, which means that when disturbance with known upper bound is added to the system, it takes more time to drive the system state to converge to a neighborhood of the origin. From (31), it can be found that a large value of the disturbance upper bound a_{pMAX} leads to a wide neighborhood; large values of θ_1 and θ_2 shrink the neighborhood size, but increase the convergence time in the meantime.

IV. Simulation Results and Analysis

In this section, three parts of simulations are presented. Firstly, the proposed guidance (25) is tested to show the effectiveness and fixed-time property. The offline fuel optimal guidance [1] is simulated to show the fuel efficiency of the proposed guidance. The super twisting method is employed to evaluate the landing rate of the proposed guidance. Secondly, disturbances are taken into consideration to test the robustness and the landing accuracy. Thirdly, the output saturation problem is considered by testing a large range of initial states.

A. Part 1: Effectiveness of the proposed guidance and fixed-time stabilization technique property test

Parameters of the lander and gravitational acceleration on Mars and Earth are listed in Table I, which are introduced in [1]. Due to the soft landing requirement, the following terminal states need to be satisfied: $\boldsymbol{r}(t_f) = \begin{bmatrix}0 & 0 & 0\end{bmatrix}^{\mathrm{T}}$ m and $\boldsymbol{v}(t_f) = \begin{bmatrix}0 & 0 & 0\end{bmatrix}^{\mathrm{T}}$ m/s.

TABLE I
Parameters of the lander

Parameters	Values
initial mass m_0	1905 kg
effective cross-sectional area $\boldsymbol{A}$	$\begin{bmatrix}6.0 & 7.5 & 8.7\end{bmatrix}^{\mathrm{T}}$ m^2
initial position $r(0)$	$\begin{bmatrix}-2000 & 1000 & 1500\end{bmatrix}^{\mathrm{T}}$ m
initial velocity $v(0)$	$\begin{bmatrix}100 & -15 & -75\end{bmatrix}^{\mathrm{T}}$ m/s
gravitational acceleration of Mars $\boldsymbol{g}$	$\begin{bmatrix}0 & 0 & -3.7114\end{bmatrix}^{\mathrm{T}}$ m/s^2
gravitational acceleration of Earth $\boldsymbol{g}_e$	$\begin{bmatrix}0 & 0 & -9.807\end{bmatrix}^{\mathrm{T}}$ m/s^2

TABLE II
Positions, Velocity and Mass With Initial Perturbations

Parameters	Mean Value	Standard dev.
Crossrange Position r_x	-2000(m)	100(m)
Downrange Position r_y	1000(m)	100(m)
Altitude Position r_z	1500(m)	100(m)
Crossrange Velocity v_x	100(m/s)	10(m/s)
Downrange Velocity v_y	-15(m/s)	10(m/s)
Altitude Velocity v_z	-75(m/s)	10(m/s)
Mass m	1905(kg)	20(kg)

TABLE III
Positions, Velocity and Mass With Initial Perturbations

Parameters	Minimum Value	Maximum Value
Crossrange Position r_x	-1000(m)	200(m)
Downrange Position r_y	0(m)	2000(m)
Altitude Position r_z	1000(m)	1500(m)
Crossrange Velocity v_x	-15(m/s)	45(m/s)
Downrange Velocity v_y	-100(m/s)	0(m/s)
Altitude Velocity v_z	-75(m/s)	0(m/s)

The simulation results of the proposed guidance are shown in Fig. 2. From Fig. 2(a), it can be seen that the proposed guidance can steer the lander to the target landing site with a high accuracy, and there is no chattering phenomenon owing to the no-switching-term reaching law design. Note that Fig. 2(a) can also be treated as the first sliding surface convergence process, because $\boldsymbol{s}_1 = \boldsymbol{r} - \boldsymbol{r}_d$ with $\boldsymbol{r}_d = 0$. From 2(b), we can

find that the velocity of the lander converges to zero finally, which satisfies the soft landing requirement. The command thrust is shown in 2(c), and the maximum value is less than 4×10^4N. Therefore, although exponential terms are employed in the proposed guidance, there is no overlarge thrust command input if proper parameters are set.

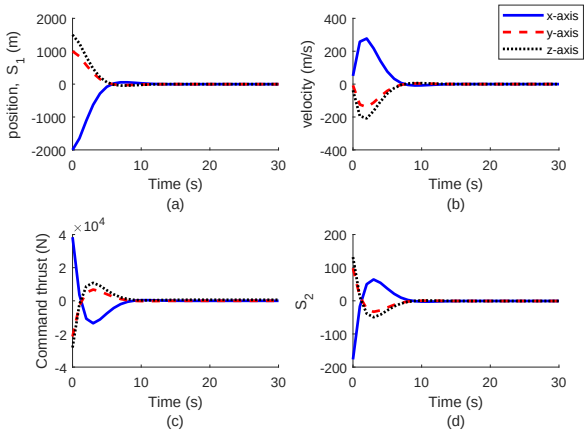

Fig. 2. Position (a), velocity (b), command thrust (c) and second sliding mode (d) with the proposed guidance

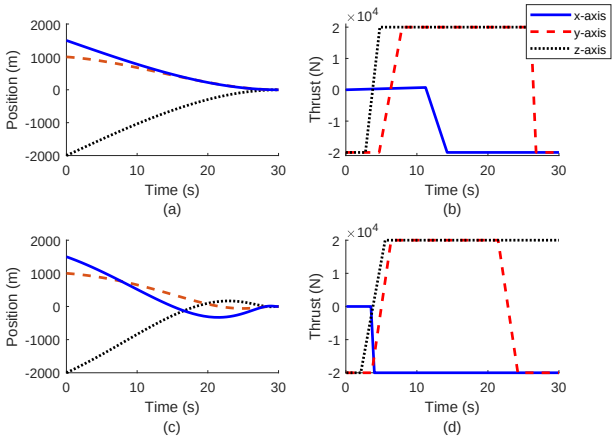

Fig. 3. Position (a) and thrust (b) without disturbances and position (c) and thrust (d) with $a_{pi} = sin(t)\text{m/s}^2$

In order to test the fuel usage of the proposed guidance, we do the simulation on the offline optimal guidance for comparison purpose. We use GPOPS to obtain an optimal solution. The whole flight time is set as $t_f = 30$s. When the disturbance is not added to the dynamic model, the position of the lander with the offline optimal guidance is shown in Fig. 3(a). It can be found from Fig. 4 that the offline optimal guidance consumes 212.9067 kg fuel and the proposed guidance consumes 238.2907 kg fuel. The thrusts of the lander using the offline optimal guidance is shown in Fig. 3(b). When the disturbance $a_{pi} = sin(t)\text{m/s}^2$, $i = x, y, z$ is added, the position of the lander with the offline optimal guidance is shown in Fig. 3(c). It can be found from Fig. 3(c) that the collision occurs with the offline optimal guidance, while with the proposed guidance, the altitude of the lander is positive. The thrusts of the lander using the offline optimal guidance are shown in Fig. 3(d). Thus, compared with the offline optimal guidance, the proposed guidance can ensure a precision landing with an acceptable fuel usage when the lander is subject to disturbances.

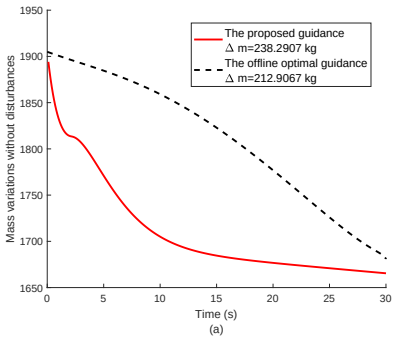

Fig. 4. Mass variations with the proposed guidance and the offline optimal guidance

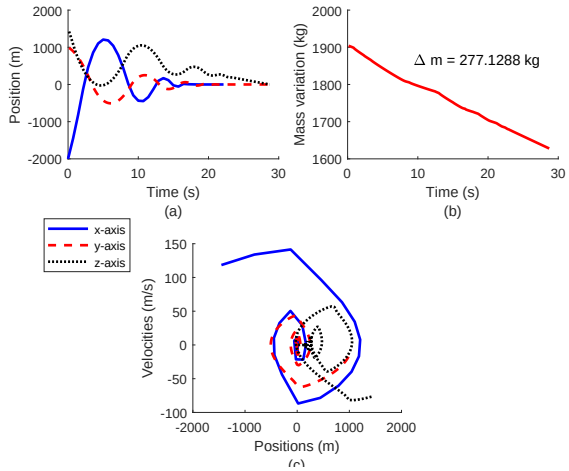

Fig. 5. Position (a), mass variation (b) and state convergence trajectories (c) with STSMG

In order to test the landing speed, we do simulation on the STSMG [16] for comparison purpose,which is designed as

$$\boldsymbol{a} = -\frac{1}{m}\{\frac{\boldsymbol{B}_1}{2}|\boldsymbol{s}|^{-\frac{1}{2}}\dot{\boldsymbol{s}} + \boldsymbol{B}_2\text{sgn}(\boldsymbol{s})\} - \boldsymbol{g} \tag{46}$$

where m denotes the mass of the lander, $\boldsymbol{s} = \begin{bmatrix} s_x & s_y & s_z \end{bmatrix}^{\text{T}}$ is the position, s_x, s_y and s_z are position components associated with x, y and z axes.The same initial states and parameters of the lander are used. The parameters of the STSMG are $\boldsymbol{B}_1 = \begin{bmatrix} 1200 & 1000 & 1000 \end{bmatrix}^{\text{T}}$ and $\boldsymbol{B}_2 = \begin{bmatrix} 5500 & 5000 & 5000 \end{bmatrix}^{\text{T}}$.

The simulation results about the STSMG are shown in Fig. 5. STSMG can ensure the lander to achieve a soft landing in 30s, which is longer than the convergence time shown in Fig. 2(a). Fig. 5(b) shows the fuel consumption with the STSMG. It can be found that 277.1288 (kg) fuel is used, which is more

than that in Fig. 4(a). Therefore, we conclude that compared with STSMG, the proposed guidance has a faster convergence speed but with less fuel consumption.

Next, we do the simulation to test the fixed-time stabilization property of the proposed guidance. From (18) and (26), the upper bounds of the convergence time can be calculated, which are $T_1 \leq 74.5780$ s in the first sliding mode for any initial states $\boldsymbol{s}_1$ and $T_2 \leq 30.8217$ s in the second sliding mode for any initial states $\boldsymbol{s}_2$, respectively. Thus, for the whole mission, the maximum time is 74.5780 s for any initial states. Simulation results of the upper bound of the convergence time T_1 and T_2 are illustrated in Fig. 6(a) and Fig. 6(b). Since three axes components have the similar regularity, we only display x-axis components of $\boldsymbol{s}_1$ and $\boldsymbol{s}_2$ to show the same time upper bound with a range of initial states $s_{1x} = -8000, -6000, -4000, -2000, -1000$ m. The convergence time of different initial values of s_{1x} is less than the calculated upper bound $T_1 \leq 74.5780$ s and the convergence time of different initial value of s_{2x} is less than the calculated upper bound $T_2 \leq 30.8217$ s. This property can meet the need of convergence rate during Mars powered descent phase, especially when the initial position and velocity of the lander are large, which is likely to happen, because the previous stage is control-free parachute phase.

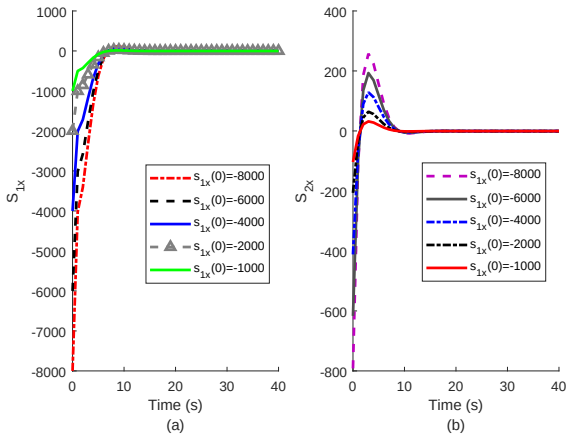

Fig. 6. S_{1x} (a) and S_{2x} (b) with different initial values

B. Part 2: Robustness of the proposed guidance and proposed practical fixed-time stabilization technique test

This part of simulation demonstrates the robustness of the proposed guidance by Monte Carlo method with 300 cases. Initial perturbations are listed in Table II. The main property of Mars is its unique atmosphere and dust storms, which are fully considered. So in this part of simulation, the harsh environment of the dust storm is chosen to be simulated to test the proposed guidance. All the unknown disturbances including the model uncertainties, atmospheric dispersions and dust storms are lumped into one disturbance term in simulation, which is expressed as:

$$a_{pi} = 20sin(t)\mathrm{m/s}^2, i = x, y, z \tag{47}$$

We set $\theta_1 = 0.2$ and $\theta_2 = 0.1$. In Fig. 7(a), the trajectories of the lander with disturbances and perturbations are shown, which all reach the target landing site eventually. The components of the velocity along three axes are shown in Figs. 7(b)∼(d). The disturbance acceleration influences the velocity trajectory dramatically, but the velocity is eventually within a neighborhood of the equilibrium point $\boldsymbol{v} = 0$ m/s. From the proposed practical fixed-time stabilization theorem $Theorem$ 1 and $Theorem$ 3, it can be calculated that the maximum final position error is 23.8472 (m) along each axis, which is verified by Fig. 8(a) and Fig. 8(b). Under disturbances and initial perturbations, the lander can achieve a near precision landing, and the maximum landing error can be calculated when the disturbance upper bound is known. It should be pointed out that collisions may occur due to disturbances, because of some negative values of r_z shown in Fig. 8(b). However, from Fig. 8(c) and Fig. 8(d), we can see that the lander crashes on the Martian surface with 1.5(m/s) as its the maximum velocity, which can also be classified as a soft landing (if the impact velocity is less than 3m/s [10], [1]).

According to the proposed $Theorem$ 3, three axes components of the second sliding surface converge within a neighborhood of the origin $s_{2i} = 0$ in a fixed time, where $i = x, y, z$, and the neighborhood can be calculated by (39) and the time can be calculated by (40), which are 26.5257 m and 131.5173 s, respectively, which are verified by Fig. 9. Similarly, from the proposed $Theorem$ 3, we can see that three axes components of the first sliding surface, which is also the position of the lander, converges within a neighborhood of the origin $s_{1i} = 0$ in a fixed time, and the neighborhood can be obtained by (31) and the time can be calculated by (45), which are 23.8472 m and 85.8610 s respectively. The simulation result shown in Fig. 10 confirms this conclusion that the system state s_{1i} can be within a boundary, which is ± 23.8472 after 9.76 s.

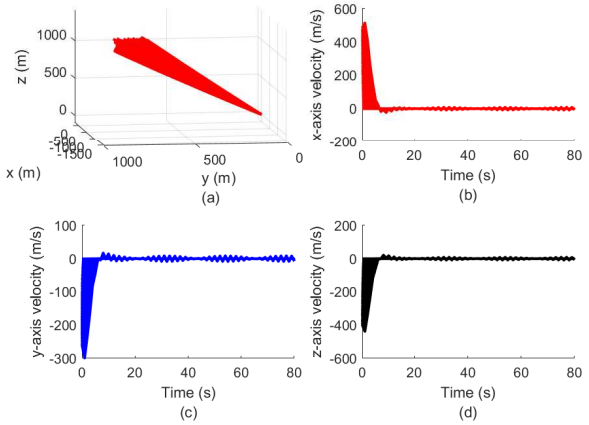

Fig. 7. Trajectories and velocities in 300 cases: (a) 3D trajectories, (b) x-axis velocity, (c) y-axis velocity, (d) z-axis velocity

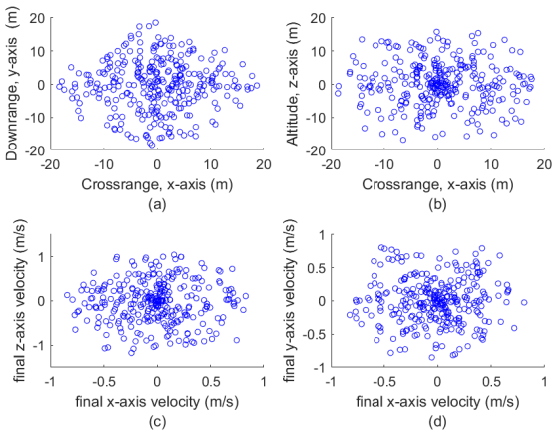

Fig. 8. Final landing sites and velocities in 300 cases: (a) landing sites on XOY plane, (b) landing sites on XOZ plane, (c) final velocities on XOZ plane, (d) final velocities on XOY plane

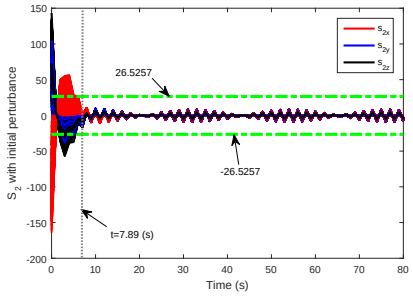

Fig. 9. Three axes s_2 vs time in 300 cases

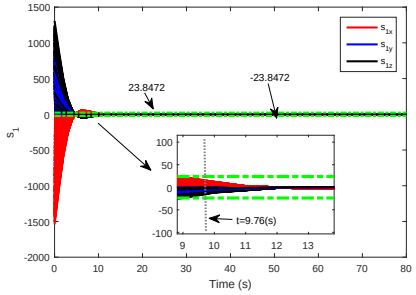

Fig. 10. Three axes s_1 vs time in 300 cases

C. Part 3: Proposed Guidance Performance With Thrust Limitation

For a lander equipped with engine-limited thrusters, it is necessary to investigate how a guidance scheme performs with this limitation [23]. The proposed guidance is based on the fixed-time stabilization technique, which needs a large control input to guarantee the convergence speed when initial states are far away from the equilibrium point. Thus, this part is to test a large range of initial positions and velocities of the lander to determine the practicability of the proposed guidance.

We test 50 cases with random initial positions and velocities, and the range of the initial positions and velocities are listed in Table III. The thrust limitation along three axes is 50000 N [1]. The positions and thrusts of the lander along three axes are shown in Figs. 11 and 12.

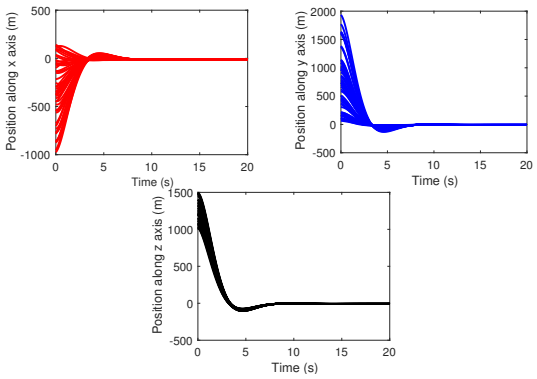

Fig. 11. Positions of the lander vs time in 50 cases

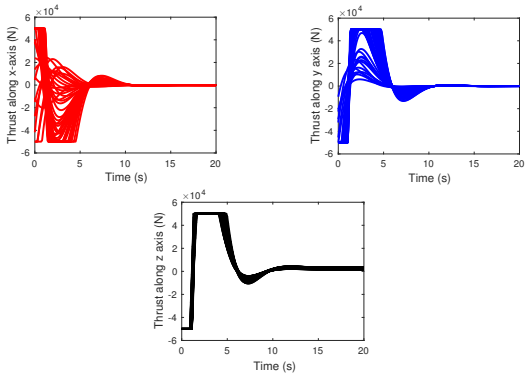

Fig. 12. Thrusts of the lander vs time in 50 cases

Fig. 11 shows that the proposed guidance can drive the lander to the target landing site with any initial positions and the convergence time is always within 10 s, which is less than the calculated upper bound. Thrusts are shown in Fig. 12, which demonstrates that the proposed guidance is still effective with thrust limitations.

V. CONCLUSIONS

This paper proposes a novel autonomous precision landing guidance scheme by employing a fixed-time stabilization technique and multiple sliding surfaces. The proposed guidance can ensure the lander to achieve a precision landing constrained by soft landing requirements within a fixed time upper bound, which is independent on initial states. Compared with offline fuel optimal guidance, the collisions can be avoided subject to the disturbance with acceptable fuel assumption. Compared with the STSMG, the proposed guidance has a faster convergence speed and consumes less fuel. The robustness of the proposed guidance is analyzed via the proposed theorem, and the maximum landing error and the upper bound of the convergence time are given. Simulation results show the fuel efficiency of the proposed guidance, and

the robustness is tested by Monte Carlo method with 300 cases. The thrust limitation is considered and the simulation results show that the proposed guidance control input is reasonable and acceptable in practical missions.

REFERENCES

[1] ACIKMESE, B., AND PLOEN, S. R. Convex programming approach to powered descent guidance for mars landing. *Journal of Guidance Control and Dynamics 30*, 5 (2007), 1353–1366.

[2] ACIKMESE, B., SCHARF, D., BLACKMORE, L., AND WOLF, A. Enhancements on the convex programming based powered descent guidance algorithm for mars landing. *Aiaa Journal* (2008).

[3] BETTANINI, C., ESPOSITO, F., DEBEI, S., MOLFESE, C., RODRIGUEZ, I. A., COLOMBATTI, G., HARRI, A. M., MONTMESSIN, F., WILSON, C., AND ABOUDAN, A. The dreams experiment on the exomars 2016 mission for the study of martian environment during the dust storm season. In *IEEE International Workshop on Metrology for Aerospace* (2014), pp. 167–173.

[4] BHAT, S. P., AND BERNSTEIN, D. S. Continuous finite-time stabilization of the translational and rotational double integrators. *IEEE Transactions on Automatic Control 43*, 5 (1998), 678–682.

[5] BLACKMORE, L., ACIKMESE, B., AND SCHARF, D. P. Minimum-landing-error powered-descent guidance for mars landing using convex optimization. *Journal of Guidance Control and Dynamics 33*, 4 (2010), 1161–1171.

[6] BRUINSMA, S., AND LEMOINE, F. G. A preliminary semiempirical thermosphere model of mars: Dtm-mars. *Journal of Geophysical Research Atmospheres 107*, E10 (2002), 15–1–15–13.

[7] DE CROON, G., ALAZARD, D., AND IZZO, D. Controlling spacecraft landings with constantly and exponentially decreasing time-to-contact. *IEEE Transactions on Aerospace and Electronic Systems 51*, 2 (2015), 1241–1252.

[8] FURFARO, R., CERSOSIMO, D., AND WIBBEN, D. R. Asteroid precision landing via multiple sliding surfaces guidance techniques. *Journal of Guidance Control and Dynamics 36*, 4 (2013), 1075–1092.

[9] FURFARO, R., WIBBEN, D. R., GAUDET, B., AND SIMO, J. Terminal multiple surface sliding guidance for planetary landing: Development, tuning and optimization via reinforcement learning. *The Journal of the Astronautical Sciences 62*, 1 (2015), 1–27.

[10] GASKELL, R. W., BARNOUIN-JHA, O. S., SCHEERES, D. J., KONOPLIV, A. S., MUKAI, T., ABE, S., SAITO, J., ISHIGURO, M., KUBOTA, T., AND HASHIMOTO, T. Characterizing and navigating small bodies with imaging data. *Meteoritics and Planetary Science 43*, 6 (2008), 1049–1061.

[11] GREELEY, R., WHITE, B. R., POLLACK, J. B., IVERSON, J. D., AND LEACH, R. N. Dust storms on mars: Considerations and simulations.

[12] GUO, Y., HAWKINS, M., AND WIE, B. Applications of generalized zero-effort-miss/zero-effort-velocity feedback guidance algorithm. *Journal of Guidance, Control, and Dynamics* (2013).

[13] GUO, Y., HAWKINS, M., AND WIE, B. Waypoint-optimized zero-effort-miss/zero-effort-velocity feedback guidance for mars landing. *Journal of Guidance, Control, and Dynamics* (2013).

[14] HUANG, X., CUI, H., AND CUI, P. An autonomous optical navigation and guidance for soft landing on asteroids. *Acta Astronautica 54*, 10 (2004), 763–771.

[15] JUSTUS, C. G., JAMES, B. F., BOUGHER, S. W., BRIDGER, A. F. C., HABERLE, R. M., MURPHY, J. R., AND ENGEL, S. Mars-gram 2000: A mars atmospheric model for engineering applications. *Advances in Space Research 29*, 2 (2002), 193–202.

[16] LEVANT, A. Sliding order and sliding accuracy in sliding mode control. *International journal of control 58*, 6 (1993), 1247–1263.

[17] LEVANT, A. Principles of 2-sliding mode design. *Automatica 43*, 4 (2007), 576–586.

[18] LIANG, C., AND LI, Y. Robust tracking of guidance trajectory for probe pinpoint soft landing on small bodies. In *IEEE International Conference on Mechatronics and Automation* (2014), pp. 999–1004.

[19] POLYAKOV, A. Nonlinear feedback design for fixed-time stabilization of linear control systems. *IEEE Transactions on Automatic Control 57*, 8 (2012), 2106–2110.

[20] STEINFELDT, B. A., GRANT, M. J., MATZ, D. A., BRAUN, R. D., AND BARTON, G. H. Guidance, navigation, and control system performance trades for mars pinpoint landing. *Journal of Spacecraft and Rockets 47*, 1 (2010), 188–198.

[21] TU, K., MUNIR, M., MEASE, K., AND BAYARD, D. Drag-based predictive tracking guidance for mars precision landing. *Journal of Guidance Control and Dynamics 23*, 4 (2000), 620–628.

[22] WANG, J., LANZON, A., AND PETERSEN, I. R. Robust output feedback consensus for networked negative-imaginary systems. *IEEE Transactions on Automatic Control 60*, 9 (2015), 2547–2552.

[23] WIE, B., ZIMMERMAN, B., LYZHOFT, J., AND VARDAXIS, G. Planetary defense mission convepts for disrupting/pulverizing hazardous asteroids with short warning time. *Astrodynamics 1*, 1 (2017), 3–21.

[24] YANG, H., AND BAOYIN, H. Fuel-optimal control for soft landing on an irregular asteroid. *IEEE Transactions on Aerospace and Electronic Systems 51*, 3 (2015), 1688–1697.

[25] ZHANG, Y., GUO, Y., MA, G., AND ZENG, T. Collision avoidance zem/zev optimal feedback guidance for powered descent phase of landing on mars. *Advances in Space Research 59*, 6 (2017), 1514–1525.

[26] ZHENG, Y., AND CUI, H. Mars atmospheric entry guidance using a sensitivity method. *IEEE Transactions on Aerospace & Electronic Systems 53*, 4 (2017), 1672–1684.

Yao Zhang received her Ph. D. in Department of Control Science and Engineering, Harbin Institute of Technology in 2018. She is currently a postdoctoral researcher in Queen Mary University of London. Her research interest covers sliding mode control, model predictive control and control applications.

Ranjan Vepa obtained his Ph. D. (Applied Mechanics) from Stanford University, USA, specialising in the area of Aeroelasticity. He is currently a senior lecturer in the School of Engineering and Material Science, Queen Mary University of London since 2001. He was with NASA Langley Research Center, where he was awarded a National Research Council Fellowship and conducted research in the area of unsteady aerodynamic modeling for active control applications.

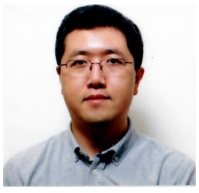

Guang Li Guang Li received the Ph.D. degree in electrical and electronics engineering, specialized in control systems, from the University of Manchester, Manchester, U.K., in 2007. He is currently a Lecturer in dynamics modeling and control with the Queen Mary University of London, London, U.K. His current research interests include constrained optimal control, model predictive control, adaptive robust control, and control applications.

Tianyi Zeng Tianyi Zeng is with the School of Automation, Beijing Institute of Technology. He has received the M.S degree in Department of Control Science and Engineering from Harbin Institute of Technology, Heilongjiang, China, in 2015. His research interest covers motor drive control and co-design of mechanism parameters and the controller.